Mixture Model for Refrigerant Pairs R-32/1234yf, R-32/1234ze(E), R-1234ze(E)/227ea, R-1234yf/152a, and R-125/1234yf

Ian H. Bell[a)]
Applied Chemicals and Materials Division, National Institute of Standards and Technology, Boulder, CO 80305, USA

(Dated: 6 December 2022)

In this work thermodynamic models based upon the corresponding states framework with departure terms are developed for the refrigerant pairs R-32/1234yf, R-32/1234ze(E), R-1234ze(E)/227ea, R-1234yf/152a, and R-125/1234yf. These models are based on new measurements of density, speed of sound, and phase equilibria, combined with the data available in the literature. The model for R-32/1234yf is most comprehensive in its data coverage, with speed of sound deviations within 1%, density deviations within 0.1%, and bubble- and dew-point pressure deviations within 1%. The other mixtures have generally more limited data availability, but a similar goodness of fit.

Keywords: hydrofluoroolefins; hydrofluorocarbons; equation of state; mixture models; refrigerants; thermodynamics

CONTENTS

LIST OF TABLES

[a)]Electronic mail: ian.bell@nist.gov

LIST OF FIGURES

I. INTRODUCTION

The increasing use of hydrofluoroolefins (HFO) to replace hydrofluorocarbons (HFC) in refrigeration applications[1] motivates the development of updated thermodynamic models for HFO-containing blends. These models are needed to carry out thermodynamic cycle analysis, design and optimize components, and so on. The previous paper in this series[2] developed a new generation of refrigerant mixture models, following in the lineage of similar efforts around the turn of the 21st century[3,4], and adding modern computational tools (evolutionary global optimization, `teqp`[5] for EOS evaluation), based upon new measurements from the National Institute of Standards and Technology (NIST).

The five binary mixtures included in this work (R-32/1234yf, R-32/1234ze(E), R-1234ze(E)/227ea, R-1234yf/152a, and R-125/1234yf) were specified in the project scope based on industrial need.

The mixture of R-32/1234yf is perhaps the most important HFO-containing binary pair for which updated parameters are needed. This binary pair yields the R-454X family of binary mixtures specified in ASHRAE standard 34[6] (the X indicating a placeholder). This binary pair also appears in other multicomponent mixtures recently added to the standard (e.g., R-448X, R-449X, R-452X, R-457X, and R-468X). The other binary mixtures described in this work also appear in blends recently added to the standard. R-32/1234ze(E) appears in the blend R-444X (and many others, see Ref. 7). R-1234ze(E)/227ea are the components of R-515B, and appears in R-471X. R-1234yf/152a appears in the blend R-457B. R-125/1234yf appears in the blend R-448B.

Information on the pure components considered in this study are included in Table I. A key point to highlight is that R-32 has a markedly higher critical pressure than the other fluids. The critical points of the pure components are shown in Fig. 1, as well as the critical curves for each of the binary mixtures from the models of REFPROP 10.0 and the models developed in this work. With the exception of R-32/1234yf, these models had no critical-point data and are thus a test of the reasonableness of the high-pressure phase equilibria behavior.

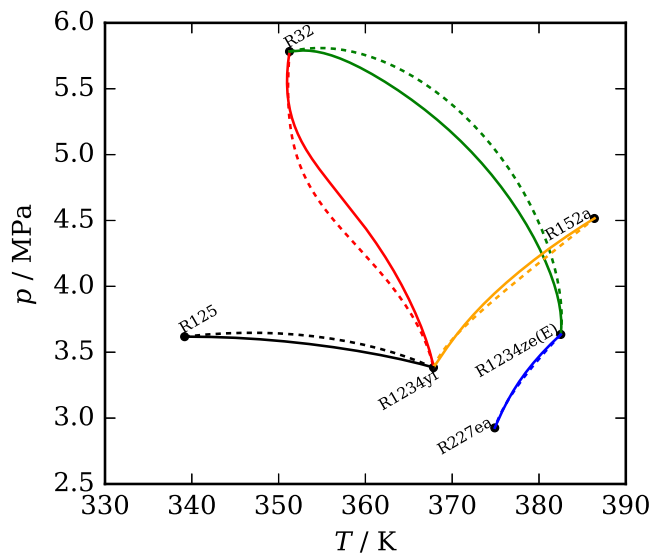

FIG. 1. Critical curves for the binary pairs in this study. Pure fluid and mixture models of REFPROP were converted to `teqp` form and integrated. The dashed curves are the REFPROP 10.0 models, and the solid curves are the models developed in this work.

II. DATA AVAILABILITY

The models developed in this work are part of a larger project on the development of new and updated thermodynamic models for HFO-containing refrigerant mixtures. The NIST measurements included:

- Density measurements with a two-sinker densimeter (all five binary pairs except for R-125/1234yf). These

TABLE I. Metadata on the pure components, sorted by normal boiling point temperature. Numerical values are taken from the respective EOS and are rounded for presentation; the unrounded value from the EOS should be used.

ASHRAE name	hash †	long name ‡	T_{NBP} / K	T_{crit} / K	p_{crit} / MPa	M / kg mol^{-1}
R-32[8]	7b05bb60	difluoromethane	221.499	351.255	5.78200	0.052024
R-125[9]	25c5a3a0	pentafluoroethane	225.060	339.173	3.61770	0.120021
R-1234yf[10]	40377b40	2,3,3,3-tetrafluoroprop-1-ene	243.692	367.850	3.38440	0.114042
R-152a[11]	63f364b0	1,1-difluoroethane	249.127	386.411	4.51675	0.066051
R-1234ze(E)[12]	9905ef70	(E)-1,3,3,3-tetrafluoropropene	254.177	382.513	3.63490	0.114042
R-227ea[13]	40091ee0	1,1,1,2,3,3,3-heptafluoropropane	256.810	374.900	2.92500	0.170029

† The hash used in REFPROP to define the unique identifier used in the mixture models is generated from the SHA256 hash of the standard InChI key from `hashlib.sha256(StdInChIkey).hexdigest()[2:9] + "0"` with the `hashlib` module from the Python standard library
‡ The long name used in REFPROP 10.0

measurements are in the gas phase and in the liquid phase

- Pulse-echo speed of sound measurements in the liquid phase (all five binary pairs)
- Bubble-point pressure measurements (all five binary pairs)

For each type of property, measurements were carried out at nominal molar compositions of 2:1 and 1:2 for each binary pair.

All other existing experimental data for these binary pairs we are aware of has been captured in NIST ThermoData Engine. NIST ThermoData Engine has a nearly comprehensive coverage of experimental data captured in the last few decades in the most important journals containing mixture experimental data; data provided via the NIST ThermoData Engine SRD#103a version 10.4.3 were used. Lists of references are provided below for each binary pair. The data used for model optimization are provided in the supplementary material.

III. OPTIMIZATION AND MODELS

A. Modeling

The model optimization approach used in this work is the same as in the previous paper in this series[2] and so will be covered only very briefly. The model formulation is based on the residual Helmholtz energy:

$$\alpha^{\mathrm{r}}(\tau,\delta,\mathbf{x}) = \alpha^{\mathrm{r}}_{\mathrm{CS}} + \alpha^{\mathrm{r}}_{\mathrm{dep}}, \tag{1}$$

where $\alpha^{\mathrm{r}}_{\mathrm{CS}}$ is the corresponding-states contribution given by

$$\alpha^{\mathrm{r}}_{\mathrm{CS}} = \sum_{i=1}^{N} x_i \alpha^{\mathrm{r}}_{0,i}(\tau,\delta), \tag{2}$$

with τ and δ the reduced variables defined by $\tau = T_{\mathrm{red}}(\mathbf{x})/T$ and $\delta = \rho/\rho_{\mathrm{red}}(\mathbf{x})$. The pure fluid equations of state (EOS) used in this work to obtain the pure fluid contribution $\alpha^{\mathrm{r}}_{0,i}(\tau,\delta)$ are the same as those used in REFPROP 10.0 with the exception of R-1234yf; in REFPROP 10.0 the EOS of Richter, McLinden, and Lemmon[14] was used while this work uses the new EOS from Lemmon and Akasaka[10].

The reducing function is defined by

$$Y_{\mathrm{red}}(\mathbf{x}) = \sum_{i=1}^{N} x_i^2 Y_{\mathrm{crit},i} + \sum_{i=1}^{N-1}\sum_{j=i+1}^{N} 2x_i x_j \frac{x_i + x_j}{\beta^2_{Y,ij} x_i + x_j} Y_{ij}, \tag{3}$$

where Y is the parameter of interest, either molar volume $v = 1/\rho$ or temperature T. The necessary parameters are given by

$$T_{ij} = \beta_{T,ij}\gamma_{T,ij}(T_{\mathrm{crit},i}T_{\mathrm{crit},j})^{0.5} \tag{4}$$

$$v_{ij} = \frac{1}{8}\beta_{v,ij}\gamma_{v,ij}\left(v^{1/3}_{\mathrm{crit},i} + v^{1/3}_{\mathrm{crit},j}\right)^3 \tag{5}$$

where $\beta_{T,ij}$, $\gamma_{T,ij}$, $\beta_{v,ij}$, and $\gamma_{v,ij}$ are fitted parameters. The departure contribution in Eq. (1) is given by

$$\alpha^{\mathrm{r}}_{\mathrm{dep}} = \sum_{i=1}^{N}\sum_{j=i+1}^{N} x_i x_j F_{ij} \alpha^{\mathrm{r}}_{ij}(\tau,\delta), \tag{6}$$

where F_{ij} is the scaling factor, normally equal to 1.0 if a departure term has been fitted, and zero if not.

The departure term $\alpha^{\mathrm{r}}_{ij}(\tau,\delta)$ for the ij pair is defined by exponential terms

$$\alpha^{\mathrm{r}}_{ij}(\tau,\delta) = \sum_k n_k \tau^{t_k}\delta^{d_k}\exp\left(-\mathrm{sgn}(l_k)\delta^{l_k}\right) \tag{7}$$

where sgn is the sign function, 0 for an argument of zero, 1 for positive arguments.

B. Pure fluid speed of sound

It was highlighted in Ref. 2 that the liquid-phase speed of sound for R-1234ze(E) is not well-represented by the existing EOS[12]. The pure-fluid deviations in speed of sound according to the best EOS are shown in Fig. S1 in the SI. This analysis shows that the most accurate speed of sound measurements for R-227ea and R-1234yf are reproduced to near the experimental uncertainty because they were used in model development, and that in all other cases the speed of sound measurements

show significant scatter outside the uncertainty bands of the most accurate measurements (with combined expanded uncertainties generally less than 0.1%). The EOS for R-1234ze(E) and R-32 have enough high-quality modern measurements of liquid-phase speed of sound that their refitting would result in a significantly better reproduction of the existing speed of sound measurements, as well as other caloric properties.

C. Optimization

A similar approach to the previous paper[2] was taken to optimize the model parameters, with the important change of adding the phase equilibria pressures into the optimization process. This change was particularly necessary for R-32/1234yf to better represent the bubble-point pressures measured in our group. The other types of data used in the fit are speed of sound data and density data. A comprehensive description of the optimization approach is not possible to include here, so the complete set of fitting code is provided in the supplementary material, along with the input data files, weights, error metrics, etc. to insure that the process is reproducible, although the outputs will not be, because the process is stochastic.

The bubble-point pressure is obtained as an iterative calculation starting from guess values for vapor and liquid densities and vapor-phase composition (the liquid-phase composition is specified). In this work, these guess values were obtained from REFPROP 10.0 and the `mix_VLE_Tx` function of `teqp` is used to do the iteration to solve for the bubble-point pressure given the liquid-phase composition and temperature (and with the necessary guess values). The bubble-point pressure is obtained by equating pressures of the co-existing phases, the chemical potentials of each component in both phases, and imposing the liquid-phase composition. The iteration can fail if the model at the given step is not well behaved, or if the iterations converge to the trivial solution (for which the liquid and vapor phases are at the same temperatures, densities, and compositions, which trivially satisfies the phase equilibria conditions). The problems of working with "bad" models are exacerbated by global optimization methods which explore the complete parameter space. In the case of failure, a large value is set for the deviation, penalizing "bad" models. The error term for the i-th data point that is added into the cost function summation is

$$r_{p,i} = 100 \times \left(\frac{p_i}{p_{\text{meas},i}} - 1 \right) \tag{8}$$

Plotting the cost function (the sum of each of the contributions to the cost function) as a function of the number of adjustable parameters in the fit gives a sense of how many terms should be used in the departure function. One would like a model with as few terms as possible to minimize the likelihood of non-physical behaviors and overfitting. Figure 2 shows the optimization runs, normalized by the best cost function for the binary pair. The values for $N_{\text{fitted}} = 4$ are for no terms in the departure function (just a reducing function), and two parameters (n_k and t_k) are added per term in the departure function.

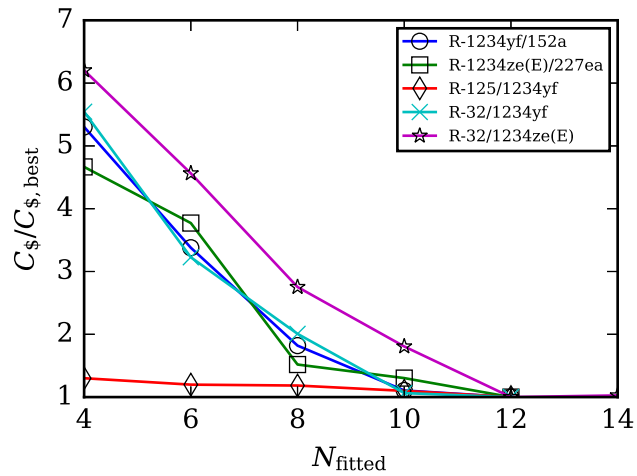

FIG. 2. Cost function history in the optimization as a function of number of fitted parameters. The best values of the cost function for each number of fitted parameters is plotted, and each pair is normalized by its best cost function value.

D. Models

Table II summarizes the interaction parameters to be used in the reducing function, and Tables III to VII summarize the coefficients that go into Eq. (7) for each binary pair. R-32/1234yf has more data available, and is one of the more asymmetric mixtures studied here.

TABLE II. Interaction parameters obtained in this work. The order matters, each pair has been sorted in increasing normal boiling point temperature order of the components

pair (1/2)	$\beta_{T,12}$	$\gamma_{T,12}$	$\beta_{v,12}$	$\gamma_{v,12}$	F_{ij}
R-32/1234ze(E)	1.005148	0.946105	0.999032	1.029821	1.0
R-32/1234yf	1.011011	0.966965	1.007852	1.037663	1.0
R-1234yf/152a	0.995987	0.978058	0.999710	1.008608	1.0
R-1234ze(E)/227ea	1.001247	0.989180	0.999290	1.001581	1.0
R-125/1234yf	0.999969	0.998028	0.998226	1.006068	1.0

TABLE III. Coefficients for the R-32/1234yf departure function.

k	n_k	t_k	d_k	l_k
0	0.449487	2.538296	1	1
1	-0.099708	3.208604	2	1
2	0.098897	0.456509	3	1

TABLE IV. Coefficients for the R-32/1234ze(E) departure function.

k	n_k	t_k	d_k	l_k
0	0.295192	0.500457	1	1
1	-0.737904	3.104735	2	1
2	0.542962	3.201720	3	1
3	-0.201951	2.567118	4	1

TABLE V. Coefficients for the R-1234yf/152a departure function.

k	n_k	t_k	d_k	l_k
0	0.009165	3.221227	1	1
1	0.014392	1.007082	2	1
2	-0.014246	3.790953	3	1

TABLE VI. Coefficients for the R-125/1234yf departure function.

k	n_k	t_k	d_k	l_k
0	-0.032013	0.00803	1	1

TABLE VII. Coefficients for the R-1234ze(E)/227ea departure function.

k	n_k	t_k	d_k	l_k
0	-0.057178	1.290298	1	1
1	0.031318	0.038796	2	1
2	-0.027496	2.640532	3	1

E. Error Metrics

The error metrics are used to quantify the goodness of fit. The deviation between an array of experimental values and an array of model-calculated values is defined by

$$\mathbf{DEV} = 100 \times \frac{\mathbf{Y}_{\text{exp}} - \mathbf{Y}_{\text{EOS}}}{\mathbf{Y}_{\text{EOS}}} \tag{9}$$

and the overall error metric (the average absolute relative deviation) is defined by

$$\text{AARD} = \text{mean}(\text{abs}(\mathbf{DEV})) \tag{10}$$

IV. RESULTS

The results for each of the studied binary pairs are included in this section. The binary pairs are presented roughly in order of confidence in the model. R-32/1234yf has been studied by many research groups and certain categories of experimental data (particularly *PTxy* data) are well studied. The remaining three binary pairs have decreasing quality and comprehensiveness of their data coverage. The last binary pair (R-1234ze(E)/227ea) is based exclusively upon new measurements carried out as part of this project; corroborative measurements from other research groups would be valuable.

A. R-32/1234yf

TABLE VIII. The collection of existing data for R-32/1234yf. (PVT: *p-v-T* data, SOS: speed of sound, VLE: vapor-liquid equilibria, *N*: number of data points, x_1: composition of the first component, CRIT: critical point , CP: constant pressure specific heat)

kind	1st author(year)	N	x_1 / mole frac.	T / K
PVT	Kobayashi(2011)[15]	295	0.35 - 0.69	310.0 - 395.0
PVT	Akasaka(2013)[16]	40	0.20 - 0.69	332.8 - 363.6
PVT	Dang(2015)[17]	26	0.48 - 0.84	283.4 - 318.6
PVT	Cai(2018)[18]	153	0.39 - 0.94	279.8 - 347.9
PVT	Yang(2019)[19]	492	0.12 - 0.87	298.8 - 383.1
PVT	Jia(2020)[20]	485	0.19 - 0.90	283.5 - 363.2
PVT	Tomassetti(2020)[21]	217	0.12 - 0.95	263.1 - 383.1
PVT	Fortin(2023)[22]	217	0.34 - 0.67	230.1 - 400.2
SOS	Shimoura(2011)[23]	92	0.63 - 0.63	283.1 - 313.1
SOS	Rowane(2022)[24]	94	0.34 - 0.67	230.0 - 345.0
VLE	Kamiaka(2010)[25]	35	0.34 - 0.84	273.3 - 333.1
VLE	Kobayashi(2011)[15]	11	0.35 - 0.69	347.8 - 359.7
VLE	Shimoura(2011)[23]	5	0.63 - 0.63	283.1 - 313.1
VLE	Kamiaka(2013)[26]	79	0.00 - 1.00	273.3 - 333.1
VLE	Hu(2017)[27]	55	0.00 - 1.00	283.1 - 323.1
VLE	Al Ghafri(2019)[28]	3	0.79 - 0.80	273.7 - 340.9
VLE	Yamada(2020)[29]	53	0.09 - 0.76	283.1 - 329.9
VLE	Li(2021)[30]	77	0.00 - 1.00	273.1 - 358.1
VLE	Outcalt(2022)[31]	30	0.37 - 0.69	270.0 - 350.0
CRIT	Kobayashi(2011)[15]	6	0.35 - 0.69	352.4 - 359.0
CRIT	Akasaka(2013)[16]	9	0.20 - 0.69	352.4 - 363.1
CP	Al Ghafri(2019)[28]	1	0.50 - 0.50	283.2 - 283.2

The mixture of R-32/1234yf is the best experimentally studied mixture of those included in this study. Although the coverage of speed of sound data remains somewhat sparse (all the mixture data are in the liquid phase), there are multiple overlapping datasets for phase equilibria and density, providing a quite good coverage of the phase diagram. The datasets are listed in Table VIII. The data in Akasaka, Tanaka, and Higashi[16] were previously presented in Akatsu, Tanaka, and Higashi[32], and the newer reference was retained as it is more broadly accessible.

The baseline mixture model from REFPROP 10.0 is based upon the EOS for R-32 from Tillner-Roth and Yokozeki[8], the EOS for R-1234yf from Richter, McLinden, and Lemmon[14], and the mixing model from Akasaka[33].

1. VLE

In total there are 9 datasets with VLE data and another with critical loci from Akasaka, Tanaka, and Higashi[16]. Most of the data cover the temperature range of practical refrigeration, and the only datasets covering the higher-temperature region are Li *et al.*[30], Kobayashi, Tanaka, and Higashi[15], and Outcalt and Rowane[34]. The measurements are largely *PTxy* where the phase compositions are obtained by sampling from the co-existing phases, an exception being that of Outcalt and Rowane[34] which are "non-invasive" bubble-point measurements for gravimetrically prepared mixtures.

Figure 3 joins all the VLE plots into one figure. The upper part of the figure is a *p-x* diagram showing the experimental data as well as traced isotherms for all of the experimentally measured temperatures. The qualitative behavior is excellent; there are no spurious wiggles or obviously physically incorrect behaviors. The isotherms were traced with the `teqp` library, starting from pure component 2. The critical locus was also traced with `teqp` with the algorithm from Deiters and Bell[35], showing that it is a Type I mixture (has a critical locus smoothly connecting the pure components). Although it is not particularly obvious in the figure, the slight dip in the R-32-rich end of the critical curve indicates that the two-phase equilibria portions of the phase diagram are separated for a very narrow range of temperatures around the critical temperature of R-32, analogous to the case of R-1234yf/134a[2].

The lower half of the figure shows the bubble- and dew-point deviations as a function of temperature and composition for this model and the model of Akasaka. The model from Akasaka[36] implemented in REFPROP 10.0 represents the experimental data available with an overall AARD in bubble-point pressure of 1.05% and an overall AARD in dew-point pressure of 1.49%. The new model improves the deviations and the AARD for the bubble-point pressures are 0.45% and 0.54% for the dew-point pressures.

The dataset of Shimoura, Matsuo, and Sotani[23] is biased systematically by approximately 10%. Otherwise, the datasets are largely in good agreement, and the data are represented to within mostly 1%, except for some of the higher temperature data from Li *et al.*[30] and a point from Al Ghafri *et al.*[28].

Overall, the data quality and availability for this binary pair appear to be suitable for the development of an accurate *PTxy* surface. The datasets appear to be largely consistent and the model reproduces the data within approximately 1% in phase equilibrium pressure.

2. PVT

As has been mentioned before[2,7], assessing the quality of fit for density data from a thermodynamic model is non-trivial. A complicating factor is that iterative solutions for density may

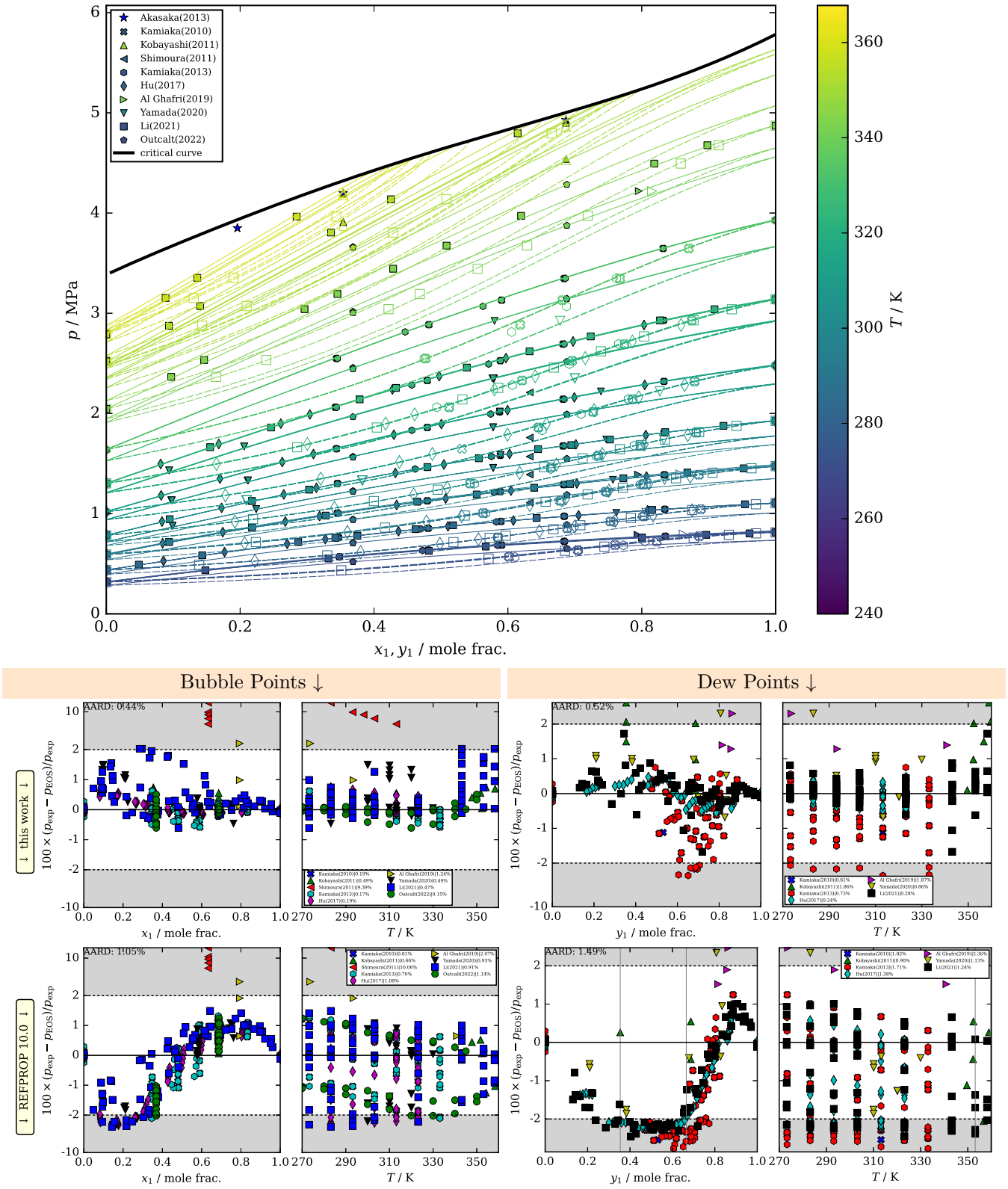

FIG. 3. VLE plots for R-32/1234yf. Experimental datasets for R-32/1234yf are listed in Table VIII. Top: A p-x diagram with points and curves colored by temperature. Bottom left: Deviation plots for bubble-point data. Bottom right: Deviation plots for dew-point data. For the deviation plots, the AARD is listed in the legend, and the portions of the plot shaded in gray are on a logarithmic scale. Thin vertical gray lines indicate values of the independent variable at the failure of an iterative calculation.

disappear as small changes are made to the model; the problem is especially pronounced for saturated state points in the critical region. Statistics of fit quality like the AARD may be deceptive because functions may become quite flat, and a large value of AARD for a density dataset does not necessarily mean that the data and model are in meaningful disagreement. Taking this preamble into account, overall density deviation plots for the model for R-32/1234yf are presented in Fig. 4. The model developed in this work yields deviations that are sometimes tens of percents in the worst case, but this error metric is deceptive, as was discussed previously[7]. The portions of the phase diagram will be investigated individually.

The gas phase has been studied by a number of groups. An expanded view of the gas-phase deviations are presented in Fig. S3 in the supplementary material. The quality of the low-density gas data and models can be assessed from the virial coefficients. The virial expansion for low-density gases reads

$$Z \equiv \frac{p}{\rho RT} = 1 + B\rho + C\rho^2 + \ldots \tag{11}$$

where B and C are the second and third virial coefficients respectively and each have composition and temperature dependence. The second virial coefficient for a binary mixture is given by

$$B(T,\mathbf{x}) = x_1^2 B_1(T) + 2x_1x_2B_{12}(T) + x_2^2 B_2(T) \tag{12}$$

where B_1 and B_2 are the second virial coefficients of the first and second component, respectively, and x are mole fractions. For each binary mixture, low-density constant-composition quasi-isothermal data allow for the calculation of $B(T,\mathbf{x})$, and given the composition, B_{12}. According to rigorous theory, the value of B_{12} should not depend on composition and thus serves as a sensitive consistency check for gas-phase isothermal data.

The derivation of B_{12} from the experimental data is more involved than it might appear at first glance. The process used in this work, including the important correction term described in Moldover and McLinden[37] is described in Section 2 in the supplementary material. The calculated values for B_{12} from the experimental gas-phase measurements of Fortin and McLinden[22] are shown in Fig. 5. The experimental data show a very small amount of scatter. The model developed in this work dramatically improves the representation of the cross second virial coefficient as compared with the model of Akasaka[36]. Both models yield a composition-dependent B_{12}, which is a consequence of the corresponding-states-based model formulation[38]. The improvement in the cross second virial coefficients is related to the improvement in the accuracy of the dew-point curve because the second virial coefficient largely governs the thermodynamics in the low-density gas.

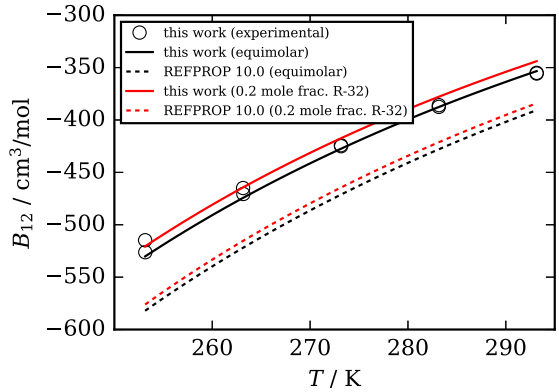

FIG. 5. Values of B_{12} for R-32/1234yf gas-phase data. Experimental data are from Fortin and McLinden[22] with the data analysis in this work, the models are the model in this work and that of the model in REFPROP 10.0.

The measurements of Cai *et al.*[18] are also quasi-isothermal measurements at constant composition in the low-density gas. Values of B_{12} were obtained from all nominal isotherms with at least 4 datapoints for a given mixture composition. The calculated values are in Fig. 6; there is an offset of approximately 50 cm^3 mol^{-1} from the values in Fig. 5 at 293.15 K. Given the consistency of the results in Fig. 5, the NIST data seem to be more reliable than those of Cai *et al.*[18]. The other low-density gas-phase datasets (Tomassetti[39] and Yang, Jia, and Wu[19]) are not amenable to the same sort of analysis.

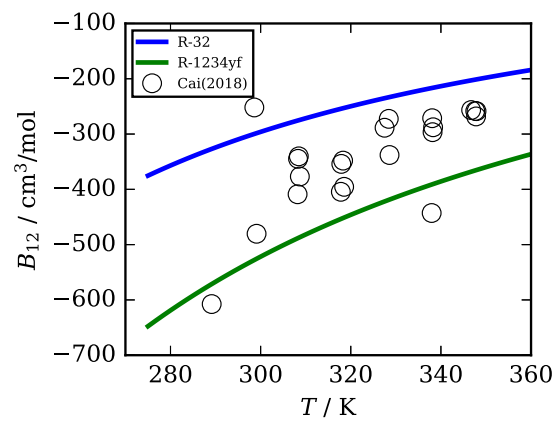

FIG. 6. Other literature values of B_{12} for low-density gas data for R-32/1234yf. Experimental data from Cai *et al.*[18]

At the other end of the phase diagram is the liquid phase, which is also well-represented by the model. In the liquid phase, here defined by $\rho > 800$ kg m^{-3}, the fit was anchored by the data from NIST, which are represented with an AARD of 0.07%. An expanded view of the liquid-phase data is shown in Fig. S4 in the supplementary material. Systematic deviations relative to the NIST data can be seen for the datasets from Dang *et al.*[17] and Jia, Yang, and Wu[20].

In between the gas-like and liquid-like densities is the extended critical region. In this region, the physics become more

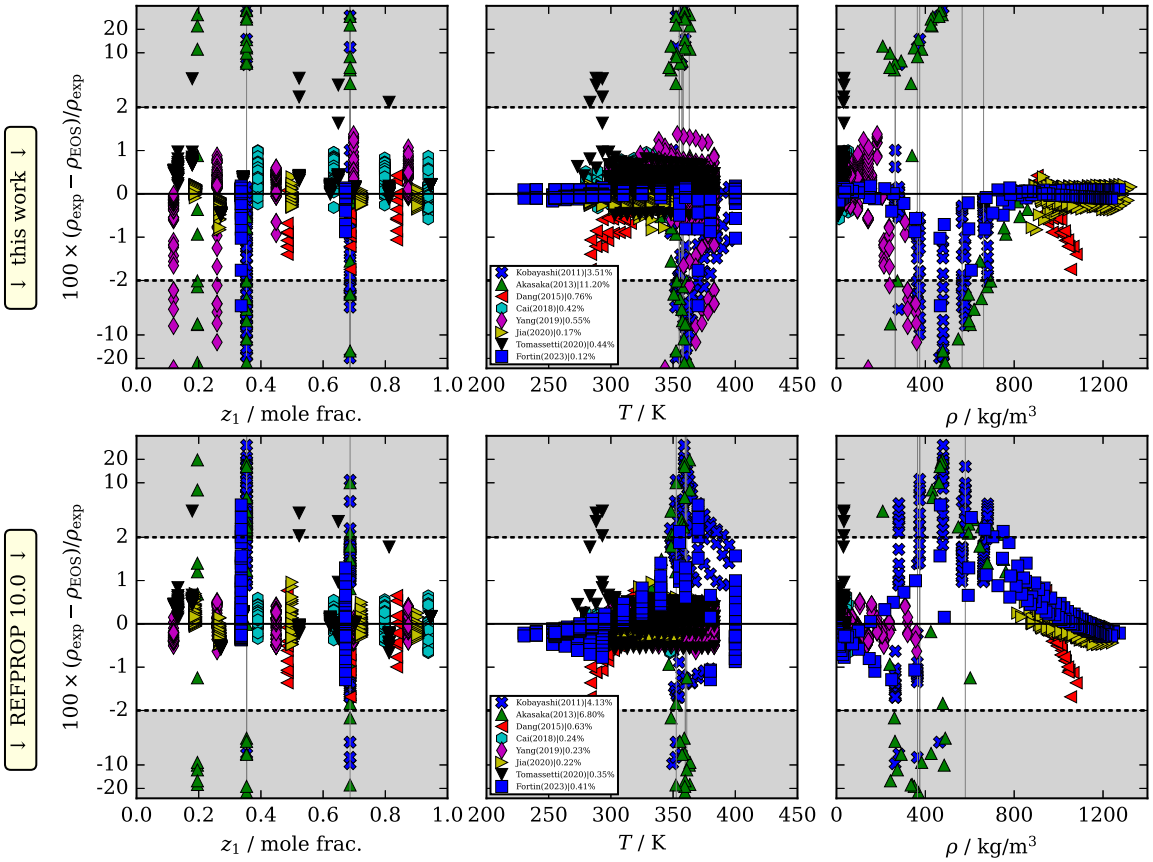

FIG. 4. PVT deviations for the model in this work and that of REFPROP 10.0 for R-32/1234yf. The references are as listed in Table VIII and the AARD for each dataset are listed in the legends. The portions of the plot shaded in gray are on a logarithmic scale. Thin vertical gray lines indicate values of the independent variable at the failure of an iterative calculation.

complicated, and the assessment of model performance for PVT data also becomes more challenging. As a demonstration of one problem, the saturated liquid and vapor density data from Akasaka, Tanaka, and Higashi[16] and the model results for the experimentally studied isopleths are shown in Fig. 7. Although the deviations are tens of percents in some cases, the performance of the model is qualitatively correct, the problem being that the isopleths are quite flat near their maximum temperature which results in large density deviations.

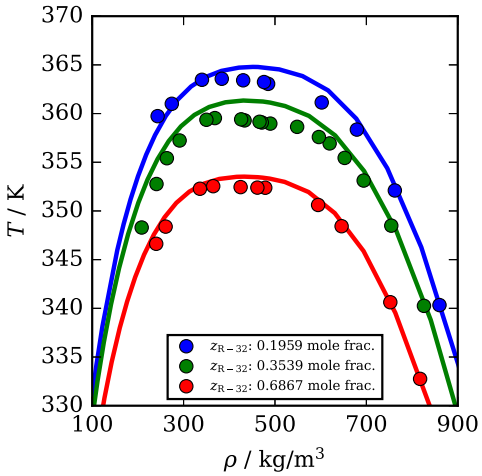

FIG. 7. Saturated isopleths for R-32/1234yf. The curves are from the new models with color matching the data points and the experimental data points for saturated phases are from Akasaka, Tanaka, and Higashi[16].

More generally, for points in the extended critical region (roughly 200 kg m^{-3} $< \rho <$ 800 kg m^{-3}), the density deviation is no longer meaningful because the derivative $(\partial\rho/\partial p)_T$

becomes very large and it is more reasonable to consider the deviations in the pressure calculated from the given temperature and density. Those results are shown in Fig. S2 in the supplementary material which show that the deviations in terms of pressure are less than 1%, which is probably as good as can be expected.

Overall the density data appear to be well captured by the model. Even though the deviation plots in Fig. 4 show some initially worrying deviations, after deeper assessment, the problems appear to be artifacts of the error metric rather than problems in the data or the model. This highlights the challenge in assessing mixture model performance: a deviation of 20% in density does not necessarily indicate fatal flaws of the model and it is only by deeper investigation that PVT deviations can be more completely understood.

3. Caloric Properties

There are two datasets for speed of sound[23,24] and a single data point of isobaric specific heat capacity c_p from Al Ghafri *et al.*[28]. Figure 8 presents the deviations for the speed of sound data. Both speed of sound datasets systematically deviate from the model of Akasaka by approximately +2%. The updated model in this work included the data from Rowane and Perkins[24] in the fit and it is therefore no surprise that the deviations of these data points are mostly within 1% with a clear temperature dependence in the deviations. The data from Shimoura, Matsuo, and Sotani[23] are likewise well-represented by the new model; the two datasets appear to be consistent. This stands in contrast to the VLE data from Shimoura, Matsuo, and Sotani[23], which deviate systematically and significantly from the other VLE data.

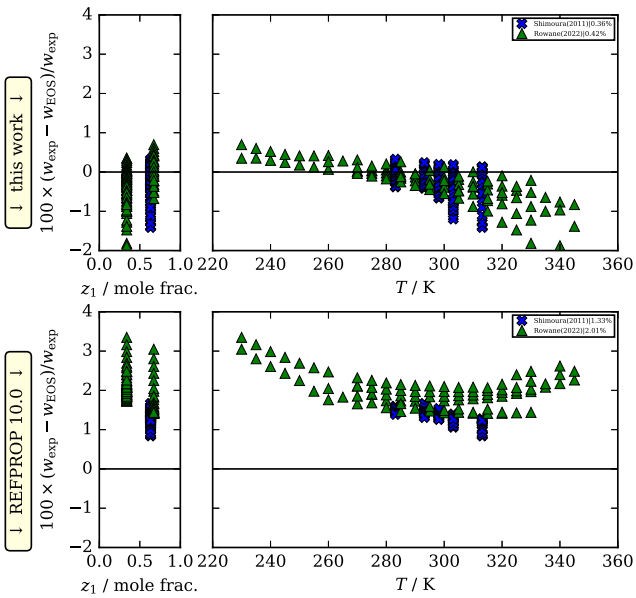

FIG. 8. Speed of sound deviations for model in this work and that of REFPROP 10.0 for R-32/1234yf. The references are as listed in Table VIII.

As was mentioned above, the deviations between the pure fluid liquid-phase speed of sound data and the respective EOS are not negligible. In the case of R-32, those deviations have a systematic trend in temperature, while the new EOS for R-1234yf largely corrects the defects in the reproduction of the pure fluid speed of sound. The mixture model probably fits the experimental speed of sound data *too* well. The deviations for pure R-32 should range from -0.25% to +0.75% in these coordinates, and R-1234yf should be represented to within near the experimental uncertainty. From the new model the limit of pure R-32 seems to be a deviation with a positive offset of approximately 0.5%.

The single datapoint for c_p is from Al Ghafri *et al.*[28]; the AARD with the new model developed in this work is 1.7% and that with the REFPROP 10.0 model is 2.1%.

B. R-32/1234ze(E)

TABLE IX. The collection of existing data for R-32/1234ze(E). (PVT: *p-v-T* data, SOS: speed of sound, VLE: vapor-liquid equilibria, N: number of data points, x_1: composition of the first component, CRIT: critical point , CP: constant pressure specific heat, CV: constant volume specific heat)

kind	1st author(year)	N	x_1 / mole frac.	T / K
PVT	Kobayashi(2010)[40]	23	0.42 - 0.69	341.2 - 371.8
PVT	Kobayashi(2011)[41]	330	0.42 - 0.69	310.0 - 400.0
PVT	Tanaka(2011)[42]	81	0.43 - 0.67	310.0 - 350.0
PVT	Yamaya(2011)[43]	47	0.70 - 0.70	280.1 - 460.1
PVT	Jia(2016)[44]	540	0.17 - 1.00	283.5 - 362.7
PVT	Tomassetti(2020)[45]	182	0.17 - 0.95	263.1 - 373.1
PVT	Fortin(2023)[22]	237	0.34 - 0.67	230.0 - 400.0
SOS	Rowane(2022)[24]	341	0.34 - 0.67	230.0 - 345.0
VLE	Kobayashi(2011)[41]	14	0.42 - 0.69	358.1 - 371.5
VLE	Tanaka(2011)[42]	10	0.43 - 0.67	310.0 - 350.0
VLE	Akasaka(2013)[33]	151	0.06 - 0.94	272.9 - 314.0
VLE	Hu(2017)[46]	65	0.00 - 1.00	283.1 - 323.1
VLE	Hu(2017)[27]	15	0.15 - 0.73	283.1 - 323.1
VLE	Kou(2019)[47]	36	0.00 - 1.00	293.1 - 323.1
VLE	Yang(2021)[48]	25	0.00 - 1.00	263.1 - 323.1
VLE	Outcalt(2022)[31]	37	0.34 - 0.64	270.0 - 360.0
CRIT	Kobayashi(2010)[40]	6	0.42 - 0.69	362.2 - 370.8
CRIT	Kobayashi(2011)[41]	6	0.42 - 0.69	362.2 - 370.8
CP	Tanaka(2011)[42]	38	0.43 - 0.67	310.0 - 350.0
CV	Yamaya(2011)[43]	47	0.70 - 0.70	280.1 - 460.1
CP	Gao(2018)[49]	25	0.23 - 0.95	310.1 - 330.1

The mixture of R-32/1234ze(E) is almost as well studied experimentally as R-32/1234yf. There are multiple overlapping datasets for phase equilibria and density, providing a quite good coverage of the phase diagram, except perhaps at extremes in temperature. The datasets are listed in Table VIII. And unlike R-32/1234yf, there are multiple datasets of specific heat measurements.

The baseline mixture model from REFPROP 10.0 is based upon the EOS for R-32 from Tillner-Roth and Yokozeki[8], the EOS for R-1234ze(E) from Thol and Lemmon[12], and the mixing model from Akasaka[33].

1. VLE

In total there are 8 datasets with VLE data and another with critical loci from Kobayashi, Tanaka, and Higashi[41], which presents the same data points as Kobayashi, Tanaka, and Higashi[40]. As for R-32/1234yf, the measurements are largely $PTxy$ where the phase compositions are obtained by sampling from the co-existing phases, but Outcalt and Rowane[34] measured VLE of gravimetrically-prepared mixtures.

Figure 9 joins all the VLE plots into one figure. The discussion largely follows that for R-32/1234yf, although the experimental data end at a lower temperature relative to the critical locus than that of R-32/1234yf. As such, there is more uncertainty in the correct shape of the critical locus. The data from Kobayashi, Tanaka, and Higashi[41] suggest that the critical locus is monotonic in pressure-composition coordinates, but neither the REFPROP 10.0 model from Akasaka[33] nor the model from this work show that behavior. The lower half of the figure shows the bubble- and dew-point deviations as a function of temperature and composition for this model and the model of Akasaka. The model from Akasaka[36] implemented in REFPROP 10.0 represents the experimental data available with an overall AARD in bubble-point pressure of 1.88% and an overall AARD in dew-point pressure of 1.80%. The new model improves the deviations and the AARD for the bubble-point pressures are 0.77% and 1.05% for the dew-point pressures. The work of Akasaka[36] also showed that the mixture models fitted to experimental data for R-32/1234ze(E) tend to have more scatter and larger deviations than those for R-32/1234yf. The origin of this scatter is unclear. Overall the datasets are largely in good agreement, and the data are represented to within mostly 2% in pressure.

Overall, the data quality and availability for this binary pair appear to be suitable for the development of an accurate $PTxy$ surface. The datasets appear to be largely consistent and the model reproduces the data within approximately 1% in phase equilibrium pressure.

2. PVT

The cross second virial coefficients are in Fig. 10. The deviations are generally within 20 cm^3/mol, except for at the lowest temperature of 253.15 K. The deviations in the low-density region are shown in Fig. S7 in the supplementary material, and are mostly within 0.05% in density.

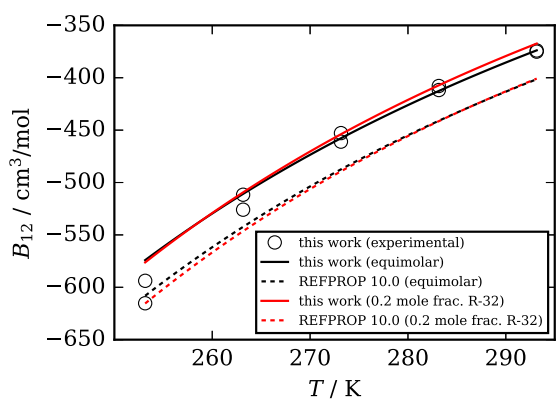

FIG. 10. Values of B_{12} for R-32/1234ze(E) gas-phase data. Experimental data from Fortin and McLinden[22] with the data analysis in this work, models are the model in this work and that of the model in REFPROP 10.0.

The liquid-phase densities are also well-represented by the model. The fit in this region was based on the NIST data, which are represented with an AARD of 0.02% and are shown in Fig. 11. An expanded view of the liquid-phase data is

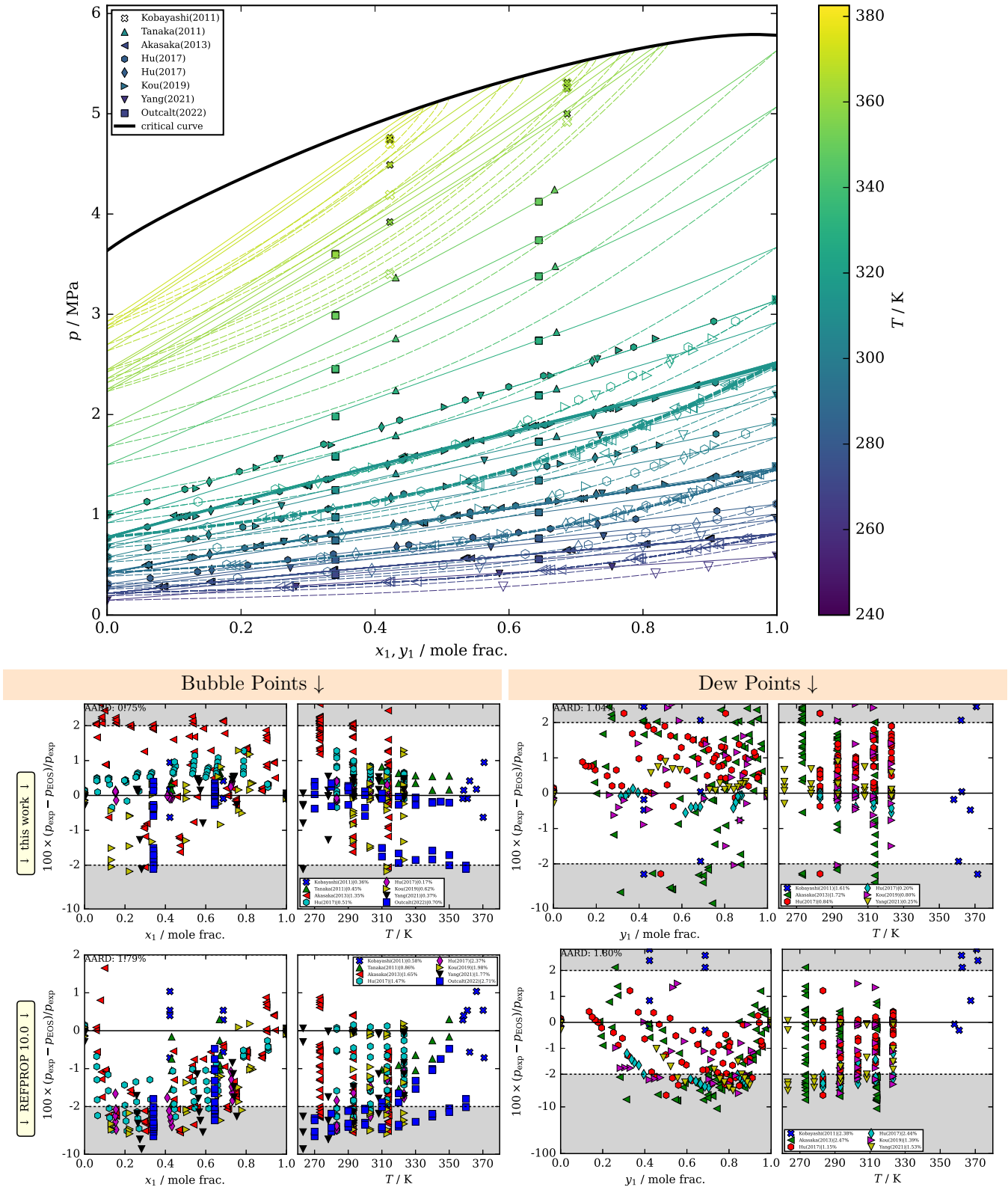

FIG. 9. VLE plots for R-32/1234ze(E). Experimental datasets for R-32/1234ze(E) are listed in Table IX. Top: A p-x diagram with points and curves colored by temperature. Bottom left: Deviation plots for bubble-point data. Bottom right: Deviation plots for dew-point data. For the deviation plots, the AARD is listed in the legend, and the portions of the plot shaded in gray are on a logarithmic scale.

shown in Fig. S7 in the supplementary material. Random deviations relative to the NIST data can be seen for the dataset from Jia *et al.*[44]. The combined expanded uncertainties of Jia *et al.*[44] are approximately 0.3% in density, and this dataset shows a systematic shift in density deviations at approximately 320 K.

The results in terms of pressure deviations in the so-called extended critical region are shown in Fig. S2 in the supplementary material showing that the deviations in pressure are less than 2%, which is probably as good as can be expected, and much smaller than deviations in terms of density.

In summary, as for R-32/1234yf, the presence of experimental measurements in the extended critical region complicates the assessment of the model quality. When considering the density in the gas and liquid phases appropriately, it is shown that the model is a faithful representation of the experimental data.

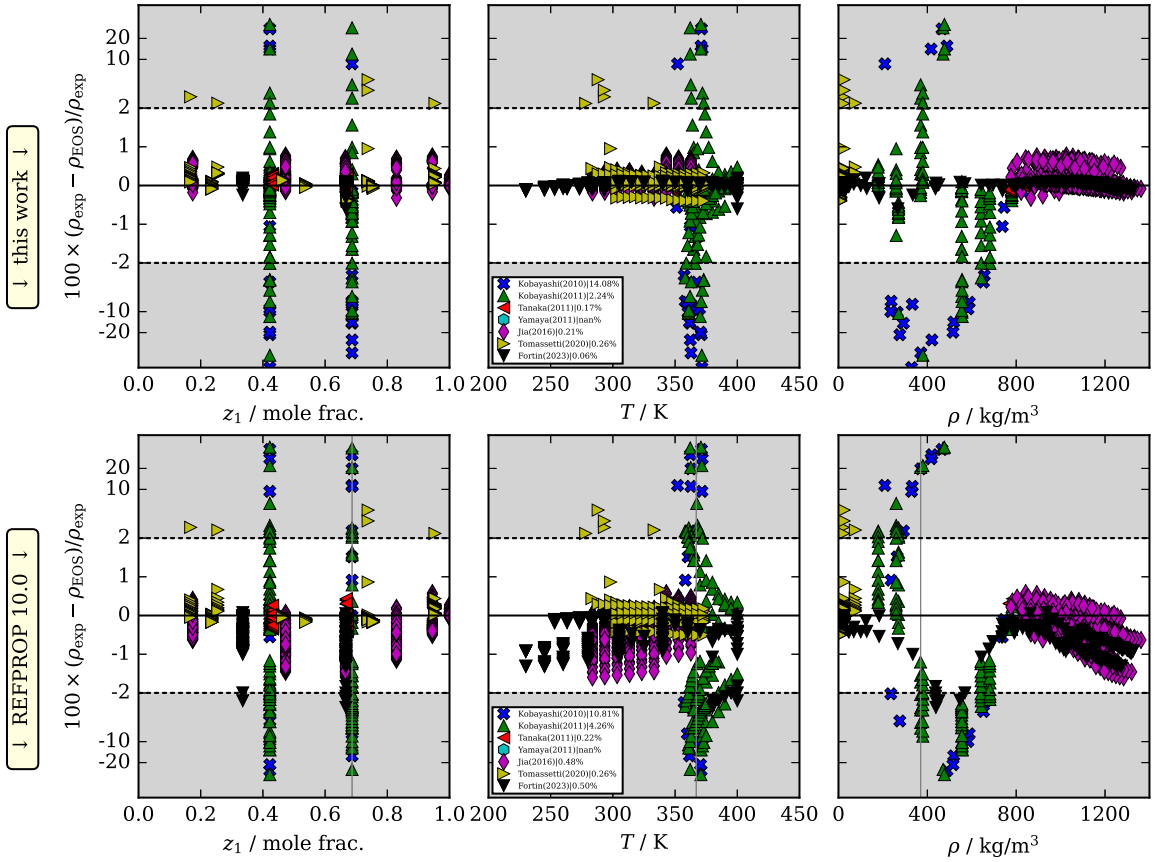

FIG. 11. PVT deviations for model in this work and that of REFPROP 10.0 for R-32/1234ze(E). The references are as listed in Table IX and the AARD for each dataset are listed in the legends. The portions of the plot shaded in gray are on a logarithmic scale. Thin vertical gray lines indicate values of the independent variable at the failure of an iterative calculation.

3. Caloric Properties

There is a single dataset of speed of sound data from Rowane and Perkins[24] and three datasets with specific heats from Tanaka, Akasaka, and Higashi[42], Yamaya, Matsuguchi, and Kagawa[43], and Gao *et al.*[49]. The coverage of specific heats is by far the most comprehensive of any of the binary pairs studied in this work.

The speed of sound deviations with the new model are shown in Fig. 12. There is no other corroborative data in the literature, so it is not possible to ascertain whether systematic deviations in the data are present. The low-temperature data were weighted more heavily in the fit such that the overall representation of the speed of sound would be improved. As was described above, the pure-fluid EOS for R-32 and R-1234ze(E) need to be refit to better reproduce the liquid-phase speed of sound.

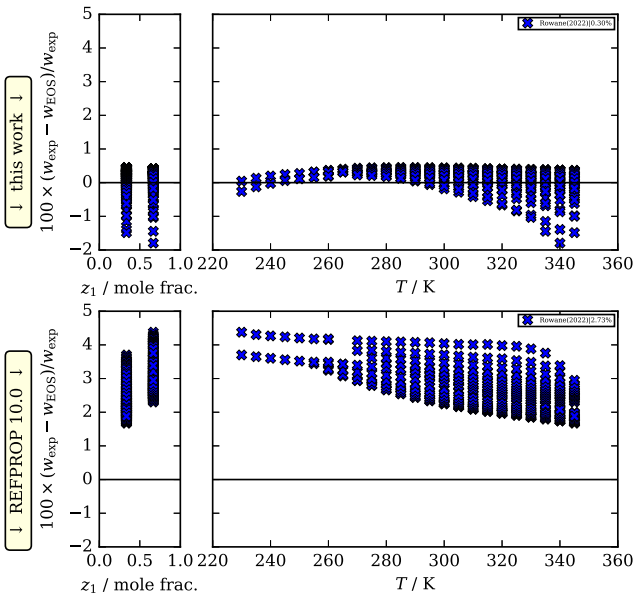

FIG. 12. Speed of sound deviations for the model in this work and that of REFPROP 10.0 for R-32/1234ze(E). The references are as listed in Table IX.

Deviation plots for the three heat capacity datasets are shown in Fig. 13 and overall the improvements in the thermodynamic model do not result in significant reductions in the deviations. Tanaka, Akasaka, and Higashi[42] claim an uncertainty of 5%, which is similar to the systematic offset of their data, and the AARD for the data of Gao *et al.*[49] is similar for the two models. The isochoric heat capacity data from Tanaka, Akasaka, and Higashi[42] extend into the critical region, causing failures of iterative routines, albeit fewer than with the model of Akasaka[36].

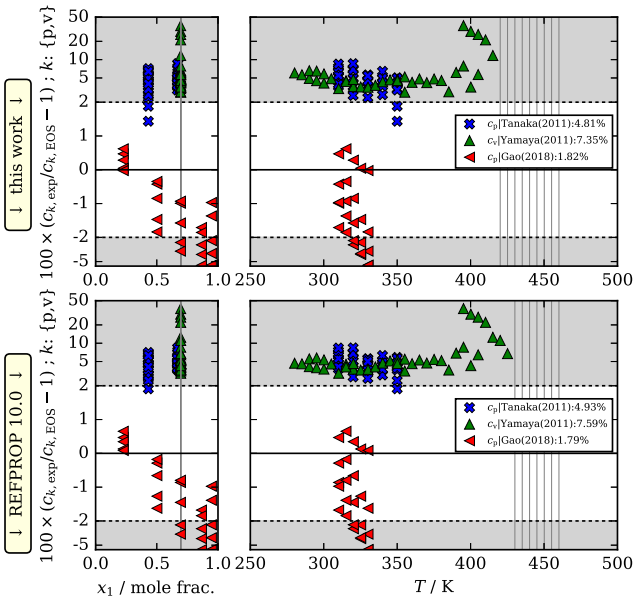

FIG. 13. Heat capacity deviations for the model in this work and that of REFPROP 10.0 for R-32/1234ze(E). The references are as listed in Table IX, and the AARD of each dataset is listed in the legend. The portions of the plot shaded in gray are on a logarithmic scale. Thin vertical gray lines indicate values of the independent variable at the failure of an iterative calculation.

C. R-1234yf/152a

The datasets from the literature for R-1234yf/152a are shown in Table X. Three of the datasets were measured in the last two years at NIST (Outcalt and Rowane[34], Rowane and Perkins[50], Fortin and McLinden[22]). Additionally, there are phase equilibria datasets measured in 2014 and 2018 (those of Hu *et al.*[51] and Yang *et al.*[52]) and a gas-phase dataset from Tomassetti[39]. The NIST datasets cover both liquid and vapor densities and the speed of sound data are liquid-phase.

TABLE X. The collection of existing data for R-1234yf/152a. (PVT: *p*-*v*-*T* data, SOS: speed of sound, VLE: vapor-liquid equilibria, N: number of data points, x_1: composition of the first component)

kind	1st author(year)	N	x_1 / mole frac.	T / K
PVT	Tomassetti(2021)[39]	161	0.13 - 0.90	263.1 - 373.1
PVT	Fortin(2023)[22]	165	0.33 - 0.67	230.0 - 400.0
SOS	Rowane(2022)[50]	138	0.33 - 0.67	230.0 - 345.0
VLE	Hu(2014)[51]	60	0.00 - 1.00	283.1 - 323.1
VLE	Yang(2018)[52]	25	0.00 - 1.00	283.1 - 323.1
VLE	Outcalt(2021)[34]	28	0.37 - 0.69	270.0 - 360.0
VLE	El Abbadi(2022)[53]	47	0.00 - 1.00	278.2 - 333.3

The baseline model from REFPROP 10.0 uses the older pure-fluid EOS for R-1234yf from Richter, McLinden, and Lemmon[14] and the same pure-fluid EOS for R-152a[11]. The mixture model in REFPROP 10.0 is based upon a simple fitting approach[7,54] yielding the interaction parameters $\beta_{T,12} = 0.9963$ and $\gamma_{T,12} = 0.98112$ with $\gamma_{v,12} = \beta_{v,12} = 1$ and $F_{ij} = 0$. The model parameters in REFPROP 10.0 are very similar to those in Table II.

1. VLE

The VLE assessment is shown in Fig. 14. The datasets from Hu *et al.*[51] and Yang *et al.*[52] are in good agreement. Both the new model from this work and the model from REFPROP 10.0 yield AARD for bubble- and dew-points less than 0.2% which is on the order of experimental uncertainty for a sampling-based $PTxy$ measurement. The dataset from Outcalt and Rowane[34] is a tale of two compositions. The composition richer in R-1234yf agrees with the other two datasets to within their mutual uncertainties. On the other hand, the composition less rich in R-1234yf shows a systematic bias on the order of 1.5%. The origin of this shift is unknown. In any case, the deviations are still less than 2%, and the corroborating data allow for a reliable mixture model. The good accuracies of the pure fluid speeds of sound are particularly helpful in this case to pin down the thermodynamics, as Ref. 2 showed that highly accurate speed of sound and *p*-*v*-*T* data can be sufficient in some cases to develop thermodynamic models without any phase equilibria data if the mixture thermodynamics are simple enough.

2. PVT

The density data cover the gas phase, the liquid phase, and some points at intermediate densities (the extended critical region). The deviations are plotted in Fig. 15. The fitted model yields excellent agreement with the experimental data used to fit it, with an AARD of 0.03% for the data from Fortin and McLinden[22] and an AARD of 0.18% for Tomassetti[39]. The model from REFPROP 10.0 does not reproduce the liquid-phase densities as well as the new model does; the REFPROP 10.0 model yields essentially unchanged statistics in the gas phase and a systematic bias of −0.25% in the liquid phase. The new model provides a good representation of the experimental density data where they exist.

The model also performs well in the dilute gas phase. The cross second virial coefficients from the data from Fortin and McLinden[22] are plotted in Fig. 16. The two models have essentially unchanged cross second virial coefficients.

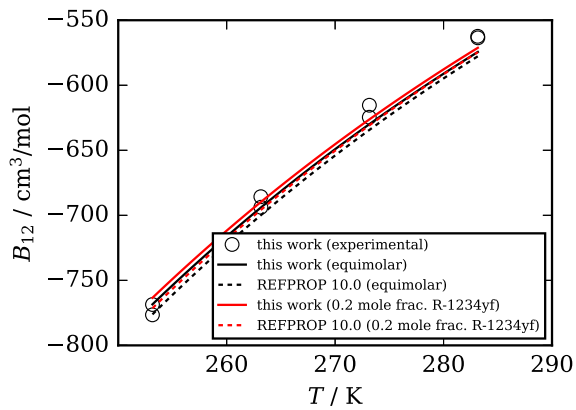

FIG. 16. Values of B_{12} for the model in this work and that of REFPROP 10.0 for R-1234yf/152a. Experimental data from Fortin and McLinden[22] with the data analysis in this work; models are the model in this work and that of the model in REFPROP 10.0.

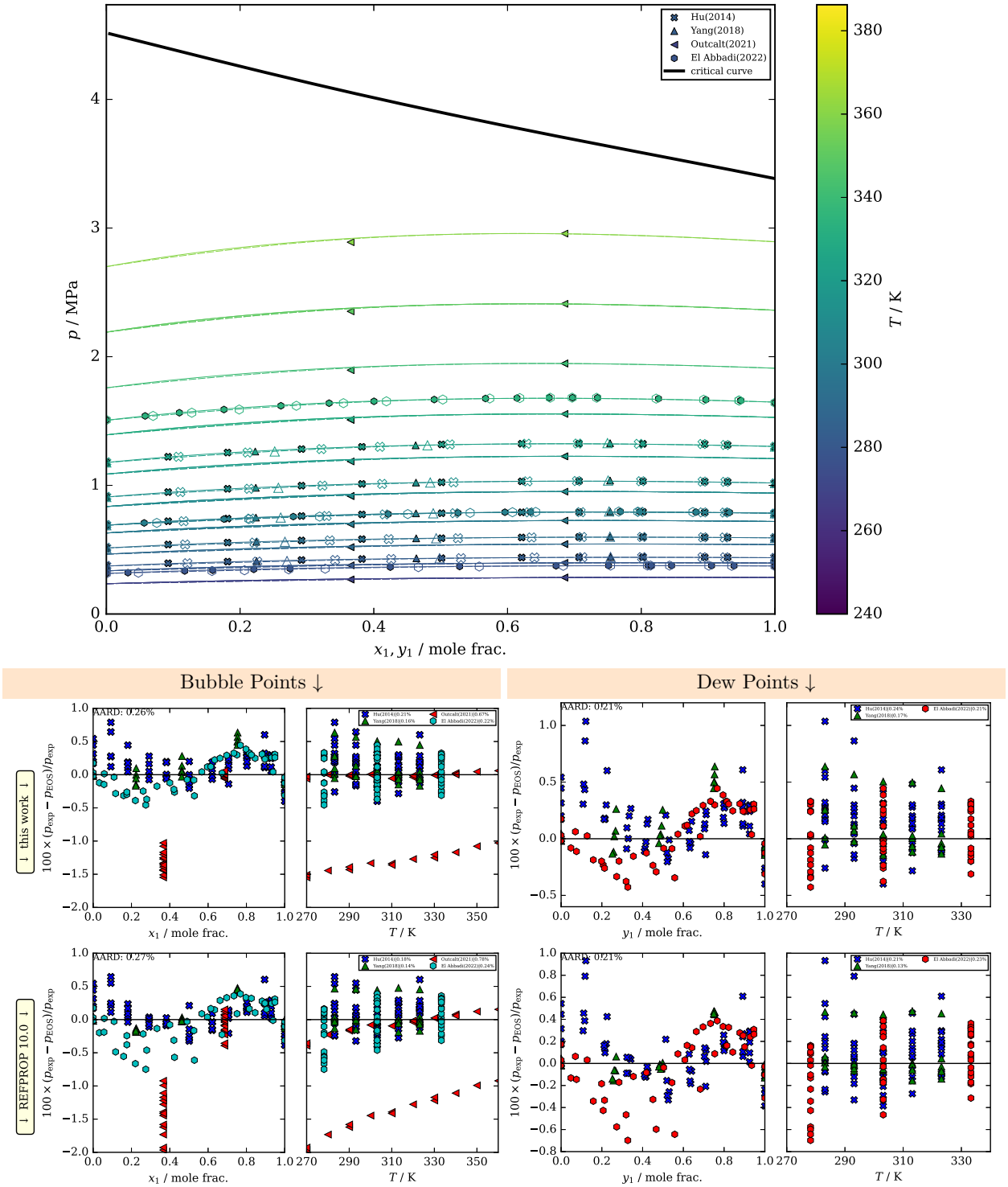

FIG. 14. VLE plots for R-1234yf/152a. The references are as listed in Table X. Top: A *p*-*x* diagram with points and curves colored by temperature. Bottom left: Deviation plots for bubble-point data. Bottom right: Deviation plots for dew-point data. For the deviation plots, the AARD is listed in the legend.

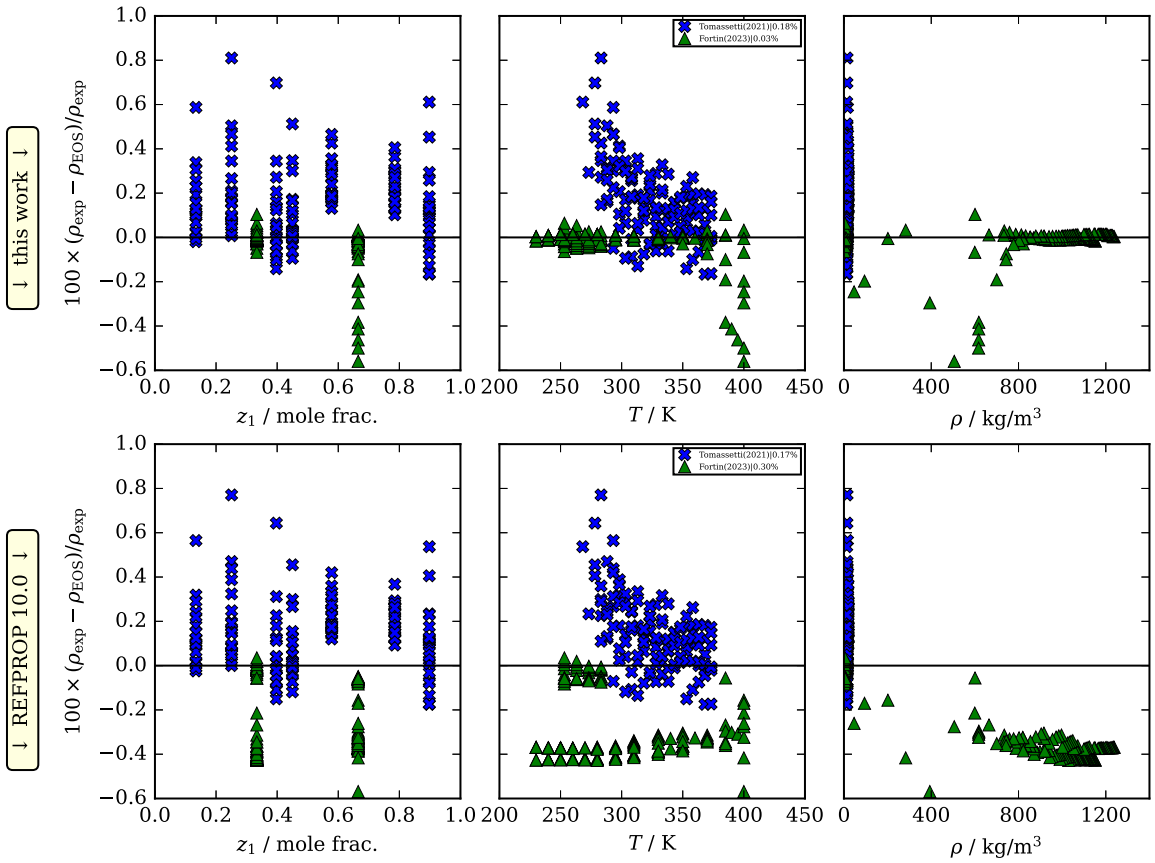

FIG. 15. Density deviations for the model in this work and that of REFPROP 10.0 for R-1234yf/152a. The references are as listed in Table X.

3. Caloric Properties

R-1234yf/152a is one of the mixtures studied in this work with a good representation of the pure-fluid speed of sound for *both* pure-fluid EOS. As a result, the highly accurate mixture speed of sound data can be used to full effect to constrain the mixture model because the mixture model does not need to correct for the erroneous pure-fluid EOS. Unsurprisingly, the representation of the mixture speed of sound after fitting is therefore also good. Figure 17 shows the deviations obtained from the model and that in REFPROP 10.0. The mixture speed of sound data are reproduced within 0.4%, with an AARD of 0.06%, which is approximately equal to the combined expanded uncertainty of the measurements. The model from REFPROP 10.0 yields much larger deviations, up to 1.5% in the worst case and an AARD of 0.35%.

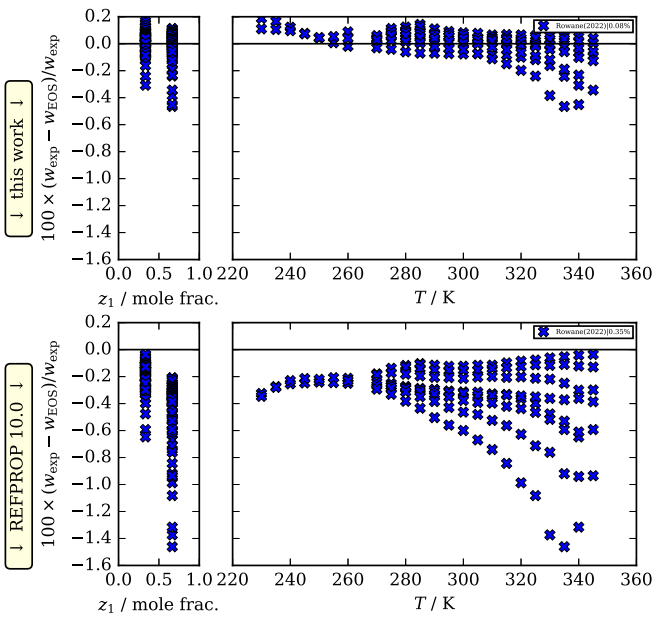

FIG. 17. Speed of sound deviations for the model in this work and that of REFPROP 10.0 for R-1234yf/152a. The references are as listed in Table X.

D. R-125/1234yf

The mixture model for R-125/1234yf is based upon VLE data from Outcalt and Rowane[34] and the speed of sound data from Rowane and Perkins[50]. The density data are used for comparison only. The existing data in the literature are summarized in Table XI.

TABLE XI. The collection of existing data for R-125/1234yf. (PVT: *p-v-T* data, SOS: speed of sound, VLE: vapor-liquid equilibria, N: number of data points, x_1: composition of the first component, CP: constant pressure specific heat)

kind	1st author(year)	N	x_1 / mole frac.	T / K
PVT	Dang(2015)[17]	27	0.29 - 0.69	283.6 - 318.0
PVT	Al Ghafri(2019)[28]	40	0.50 - 0.50	252.1 - 382.9
SOS	Rowane(2022)[50]	133	0.33 - 0.67	230.0 - 345.0
VLE	Kamiaka(2010)[25]	28	0.19 - 0.49	273.3 - 333.1
VLE	Kamiaka(2013)[26]	84	0.00 - 1.00	273.3 - 333.2
VLE	Yang(2020)[55]	35	0.00 - 1.00	283.1 - 323.1
VLE	Outcalt(2021)[34]	28	0.35 - 0.66	270.0 - 335.0
VLE	Peng(2022)[56]	66	0.00 - 1.00	263.1 - 313.1
CP	Al Ghafri(2019)[28]	1	0.50 - 0.50	293.2 - 293.2

The mixture model from REFPROP 10.0 is based upon the EOS for R-125 from Lemmon and Jacobsen[9], the EOS for R-1234yf from Richter, McLinden, and Lemmon[14], and unpublished mixing parameters[7].

The available VLE data are plotted in Fig. 18. Aside from the data from Kamiaka, Dang, and Hihara[25] and Kamiaka, Dang, and Hihara[26], the bubble-point data are represented within 0.5%. The representation of dew points is similar; the same datasets from Kamiaka, Dang, and Hihara[25] and Kamiaka, Dang, and Hihara[26] show larger deviations, and the remaining datasets are mostly represented within 0.5%. Interestingly, the updated mixture model has only a very small impact on the VLE. The critical curve traced with `teqp` is smooth and shows no anomalous behavior.

The data availability for PVT is more sparse; additional gas-phase density measurements for this mixture would be beneficial. The data in the liquid phase come from Dang *et al.*[17] and Al Ghafri *et al.*[28] and the gas-phase data come from Al Ghafri *et al.*[28]. The deviations are plotted in Fig. S8 in the supplementary material. Like the VLE, the PVT deviations are improved with the new mixture model, but only slightly.

The deviations between the experimental speed of sound data and the model are shown in Fig. S9 in the supplementary material. Like for R-1234yf/152a, the pure-fluid EOS provide good values for the speed of sound for both components, and therefore the mixture model also yields highly accurate values for the mixture speed of sound. The mixture speed of sound values are reproduced within 0.2% with an AARD of 0.1%. The mixture model from REFPROP 10.0 yields errors of up to 1.4%, with an AARD of 0.64%. The single data point for c_p is from Al Ghafri *et al.*[28]; the AARD with the new model developed in this work is 1.0% and that with the REFPROP 10.0 model is 0.9%.

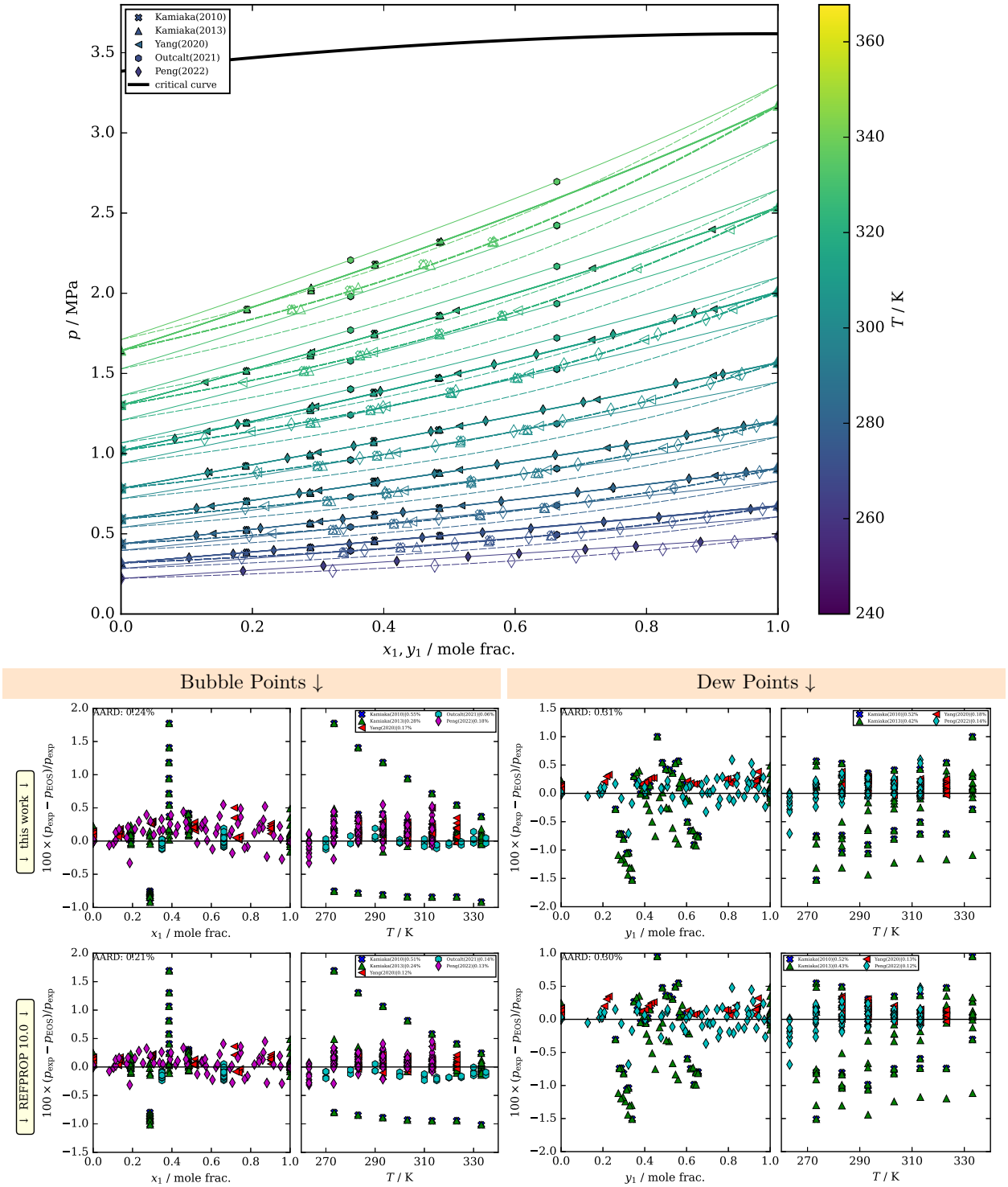

FIG. 18. VLE plots for R-125/1234yf. The references are as listed in Table XI. Top: A *p*-*x* diagram with points and curves colored by temperature. Bottom left: Deviation plots for bubble-point data. Bottom right: Deviation plots for dew-point data. For the deviation plots, the AARD is listed in the legend.

E. R-1234ze(E)/227ea

The data for R-1234ze(E)/227ea used for model development all come from new measurements conducted at NIST and the datasets are summarized in Table XII. All the data were used in the model fitting, and as a consequence, all the data are well-represented by the model. Because of the limited data coverage, the figures have been placed in the supplementary material and the data analysis is presented here.

TABLE XII. The collection of existing data for R-1234ze(E)/227ea. (PVT: *p*-*v*-*T* data, SOS: speed of sound, VLE: vapor-liquid equilibria, N: number of data points, x_1: composition of the first component)

kind	1st author(year)	N	x_1 / mole frac.	T / K
PVT	Fortin(2023)[22]	164	0.33 - 0.67	230.0 - 400.0
SOS	Rowane(2022)[50]	313	0.33 - 0.67	230.0 - 345.0
VLE	Outcalt(2021)[34]	29	0.33 - 0.68	270.0 - 360.0

The model in REFPROP 10.0 for the binary pair is the pure-fluid EOS for R-1234ze(E) of Thol and Lemmon[12] and the pure-fluid EOS for R-227ea of Lemmon and Span[13], and the mixture model uses the parameters from R-1234yf/227ea[7,54] because no experimental data were previously available.

The bubble-point measurements show systematic deviations on the order of +2% from the model in REFPROP 10.0, whereas the new model fits the bubble-point measurements with an AARD of 0.05%. The bubble-point data were included in the fit.

The density measurements cover the full density range and are reproduced with an AARD of 0.03% and a maximum deviation of 0.5%. The density deviations from the model in REFPROP 10.0 were represented with an AARD of 0.47%, so the new model represents a significant improvement in accuracy.

The speed of sound measurements show the characteristic temperature-dependent deviations shown for all studied mixtures containing R-1234ze(E) (see Ref. 2). The deviations increase in magnitude as the amount of R-1234ze(E) increases, but are still within 1.5% for all the measurements.

V. VALIDATION AND VERIFICATION

The models presented in this work were implemented in REFPROP and `teqp`. The necessary files are provided in the supplementary material. Calculated values are provided in Table XIII, and it was confirmed that the upcoming version of REFPROP and `teqp` yielded the same results to 13 digits. The new equation of state for R-1234yf of Lemmon and Akasaka[10] is also provided in REFPROP and `teqp` formats. An updated fluid file for REFPROP for R-152a is also provided, with the coefficients rounded to agree with the original publication[11] in order to yield the precise values in the table.

VI. CONCLUSIONS

In this study, mixture models were developed for five binary pairs of varying experimental databases. The model for R-32/1234yf is based upon data from multiple overlapping datasets that are well-represented. On the other end of the spectrum is the model for R-1234ze(E)/227ea based exclusively on new data. In all cases, the models provide as good a model as can be justified without over-fitting the existing data.

As in the previous study[2], it is again highlighted that deficiencies in the pure-fluid EOS, particularly in their representation of liquid-phase speed of sound, cause difficulty in development of the highest-accuracy mixture models. If the mixture models were not overfit, the mixture models will hopefully not need to be updated when the EOS for R-32 and R-1234ze(E) are updated (but success cannot be assessed until the EOS are updated at some point in the future).

VII. SUPPLEMENTARY MATERIAL

In order to ensure reproducibility of the results, the supplementary material includes 1) the fitting code and the experimental data used in the fitting process 2) the Python code used to generate the check values as well as the fluid files needed for the new EOS for R-1234yf 3) model implementations in the formats needed for REFPROP/TREND and CoolProp/teqp. For REFPROP, this incudes the HMX.BNC file.

ACKNOWLEDGEMENTS

Thanks to Demian Riccardi (of NIST) for help accessing data of TDE. This work was partially supported by: the U.S. Department of Energy, Building Technologies Office under Agreement 892434-19-S-EE000031.

VIII. AUTHOR DECLARATIONS

A. Conflict of Interest

The author has no conflicts to disclose

IX. DATA AVAILABILITY

The supplementary material, described above, includes the data used in this study. Additional information may be obtained from the author.

X. REFERENCES

[1] M. O. McLinden and M. L. Huber, "(R)Evolution of refrigerants," J. Chem. Eng. Data. **65**, 4176–4193 (2020).

TABLE XIII. Check values for the fitted model. Values obtained with teqp[a] from nominal values of $\rho/\rho_{\mathrm{red}} = 0.8$ and $T_{\mathrm{red}}/T = 0.8$. The first set of lines are check values for the pure fluids followed by one check value per binary pair. Names match the fluid file in REFPROP, are case-sensitive, and are compatible with CoolProp and `teqp`.

names (1/2)	z_1 / mole frac.	T / K	ρ / mol/m^3	T_{red} / K	ρ_{red} / mol/m^3	α^{r}
R32	1.0	439.0	6520.0	351.2550000000000	8150.0845999999992	-0.54027465374297
NEWR1234YF	1.0	460.0	3344.0	367.8500000000000	4180.0000000000000	-0.46835370596876
R125	1.0	424.0	3823.0	339.1730000000000	4779.0000000000000	-0.45506005234449
R152A	1.0	483.0	4457.0	386.4110000000000	5571.4499999999998	-0.50742149570151
R1234ZEE	1.0	478.0	3432.0	382.5130000000000	4290.0000000000000	-0.46340978447230
R227EA	1.0	469.0	2796.0	374.9000000000000	3495.0000000000000	-0.44238576197982
R32/NEWR1234YF	0.4	445.0	4149.0	355.8223718962623	5186.1403601482143	-0.47311064743911
R32/R1234ZEE	0.4	451.0	4242.0	360.5363396425610	5302.9894479051318	-0.48576186760231
R125/NEWR1234YF	0.4	445.0	3513.0	355.9041714483963	4391.8742755801022	-0.46576307479447
NEWR1234YF/R152A	0.4	469.0	3930.0	374.8173271996727	4912.7184190598955	-0.48967548916638
R1234ZEE/R227EA	0.4	470.0	3023.0	376.0139530327517	3778.4584946374848	-0.45378834770736

a: teqp version 0.14.1

[2] I. H. Bell, "Mixture Models for Refrigerants R-1234yf/134a, R-1234yf/1234ze(E), and R-134a/1234ze(E) and Interim Models for R-125/1234yf, R-1234ze(E)/227ea, and R-1234yf/152a," J. Phys. Chem. Ref. Data **51**, 013103 (2022).

[3] E. W. Lemmon and R. T. Jacobsen, "Equations of State for Mixtures of R-32, R-125, R-134a, R-143a, and R-152a," J. Phys. Chem. Ref. Data **33**, 593–620 (2004).

[4] E. W. Lemmon and R. Tillner-Roth, "A Helmholtz energy equation of state for calculating the thermodynamic properties of fluid mixtures," Fluid Phase Equilib. **165**, 1–21 (1999).

[5] I. H. Bell, U. K. Deiters, and A. M. M. Leal, "Implementing an Equation of State Without Derivatives: teqp," Ind. Eng. Chem. Res. **61**, 6010–6027 (2022).

[6] ASHRAE, "ANSI/ASHRAE Standard 34-2019 Designation and Safety Classification of Refrigerants," (2019).

[7] I. H. Bell, D. Riccardi, A. Bazyleva, and M. O. McLinden, "Survey of data and models for refrigerant mixtures containing halogenated olefins," J. Chem. Eng. Data. **66**, 2335–2354 (2021).

[8] R. Tillner-Roth and A. Yokozeki, "An International Standard Equation of State for Difluoromethane (R-32) for Temperatures from the Triple Point at 136.34 K to 435 K and Pressures up to 70 MPa," J. Phys. Chem. Ref. Data **26**, 1273–1328 (1997).

[9] E. W. Lemmon and R. T. Jacobsen, "A New Functional Form and New Fitting Techniques for Equations of State with Application to Pentafluoroethane (HFC-125)," J. Phys. Chem. Ref. Data **34**, 69–108 (2005).

[10] E. W. Lemmon and R. Akasaka, "An International Standard Formulation for 2,3,3,3-Tetrafluoroprop-1-ene (R1234yf) Covering Temperatures from the Triple Point Temperature to 410 K and Pressures Up to 100 MPa," Int. J. Thermophys. **43** (2022), 10.1007/s10765-022-03015-y.

[11] S. L. Outcalt and M. O. McLinden, "A Modified Benedict–Webb–Rubin Equation of State for the Thermodynamic Properties of R152a (1,1-difluoroethane)," J. Phys. Chem. Ref. Data **25**, 605–636 (1996).

[12] M. Thol and E. W. Lemmon, "Equation of State for the Thermodynamic Properties of trans-1,3,3,3-Tetrafluoropropene [R-1234ze(E)]," Int. J. Thermophys. **37** (2016), 10.1007/s10765-016-2040-6.

[13] E. W. Lemmon and R. Span, "Thermodynamic Properties of R-227ea, R-365mfc, R-115, and R-13I1," J. Chem. Eng. Data **60**, 3745–3758 (2015).

[14] M. Richter, M. O. McLinden, and E. W. Lemmon, "Thermodynamic Properties of 2,3,3,3-Tetrafluoroprop-1-ene (R1234yf): Vapor Pressure and p-ρ-T Measurements and an Equation of State," J. Chem. Eng. Data **56**, 3254–3264 (2011).

[15] K. Kobayashi, K. Tanaka, and Y. Higashi, "Measurements of PρTx Properties for the Binary HFO-1234yf + HFC-32 Mixtures," in *International Congress of Refrigeration* (Prague: Czech Republic, 2011).

[16] R. Akasaka, K. Tanaka, and Y. Higashi, "Measurements of saturated densities and critical parameters for the binary mixture of 2,3,3,3-tetrafluoropropene (R-1234yf) + difluoromethane (R-32)," Int. J. Refrig. **36**, 1341–1346 (2013).

[17] Y. Dang, T. Kamiaka, C. Dang, and E. Hihara, "Liquid viscosity of low-GWP refrigerant mixtures (R32 + R1234yf) and (R125 + R1234yf)," J. Chem. Thermodyn. **89**, 183–188 (2015).

[18] X.-D. Cai, N. Zhang, L.-X. Chen, P. Hu, G. Zhao, and M.-H. Liu, "Gaseous PvTx measurements of HFO-1234yf + HFC-32 binary mixture by single-sinker magnetic suspension densimeter," Fluid Phase Equilib. **460**, 119–125 (2018).

[19] J. Yang, X. Jia, and J. Wu, "Vapor phase pvTx measurements of binary mixtures of difluoromethane (R32) and 2,3,3,3-tetrafluoroprop-1-ene (R1234yf)," J. Chem. Thermodyn. **134**, 41–51 (2019).

[20] X. Jia, J. Yang, and J. Wu, "Compressed liquid densities of binary mixtures of difluoromethane (R32) and 2,3,3,3-tetrafluoroprop-1-Ene (R1234yf) at temperatures from (283 to 363) K and pressures up to 100 MPa," J. Chem. Thermodyn. **141**, 105935 (2020).

[21] S. Tomassetti, G. Coccia, M. Pierantozzi, G. Di Nicola, and J. S. Brown, "Vapor phase and two-phase PvTz measurements of difluoromethane + 2,3,3,3-tetrafluoroprop-1-ene," J. Chem. Thermodyn. **141**, 105966 (2020).

[22] T. J. Fortin and M. O. McLinden, "Vapor and Liquid (p-ρ-T-x) Measurements of Binary Refrigerant Blends Containing R-32, R-152a, R-227ea, R-1234yf, and R-1234ze(E)," J. Chem. Eng. Data (2022 (to be submitted)).

[23] H. Shimoura, S. Matsuo, and T. Sotani, "Speed of sound measurements in dense liquid of low GWP refrigerant mixture including HFO-1234yf," in *The 32nd Japan Symposium on Thermophysical Properties* (Yokohama: Japan, 2011).

[24] A. J. Rowane and R. A. Perkins, "Speed of Sound Measurements of Binary Mixtures of Difluoromethane (R-32) with 2,3,3,3-Tetrafluoropropene (R-1234yf) or trans-1,3,3,3-Tetrafluoropropene (R-1234ze(E)) Refrigerants," Int. J. Thermophys. **43**, 46 (2022).

[25] T. Kamiaka, C. Dang, and E. Hihara, "Vapor-Liquid Equilibrium Measurements of HFC-32+HFO-1234yf and HFC-125+HFO-1234yf Refrigerant Mixture," in *JSRAE Annual Conference* (Kanazawa, 2010).

[26] T. Kamiaka, C. Dang, and E. Hihara, "Vapor-liquid equilibrium measurements for binary mixtures of R1234yf with R32, R125, and R134a," Int. J. Refrig. **36**, 965–971 (2013).

[27] X. Hu, T. Yang, X. Meng, S. Bi, and J. Wu, "Vapor liquid equilibrium measurements for difluoromethane (R32) + 2,3,3,3-tetrafluoroprop-1-ene (R1234yf) and fluoroethane (R161) + 2,3,3,3-tetrafluoroprop-1-ene (R1234yf)," Fluid Phase Equilib. **438**, 10–17 (2017).

[28] S. Z. Al Ghafri, D. Rowland, M. Akhfash, A. Arami-Niya, M. Khamphasith, X. Xiao, T. Tsuji, Y. Tanaka, Y. Seiki, E. F. May, and T. J. Hughes, "Thermodynamic properties of hydrofluoroolefin (R1234yf and R1234ze(E)) refrigerant mixtures: Density, vapour-liquid equilibrium, and heat capacity data and modelling," Int. J. Refrig. **98**, 249–260 (2019).

[29] T. Yamada, H. Miyamoto, N. Sakoda, and Y. Higashi, "Vapor-Liquid Equilibrium Property Measurements for R32/R1234yf Binary Mixtures in Low R32 Concentration," Int. J. Thermophys. **41**, 167 (2020).

[30] S. Li, S. Peng, Z. Yang, and Y. Duan, "Measurements and correlation of vapor-liquid equilibrium for difluoromethane (R-32) + 2,3,3,3-

tetrafluoroprop-1-ene (R-1234yf) and pentafluoroethane (R-125) + propane (R-290)," Fluid Phase Equilib. **538**, 113010 (2021).

[31]S. Outcalt and A. Rowane, "Bubble Point Measurements of Three Binary Mixtures of Refrigerants: R-32/1234yf, R-32/1234ze(E) and R1132a/1234yf," J. Chem. Eng. Data **67**, 932–940 (2022).

[32]M. Akatsu, K. Tanaka, and Y. Higashi, "Measurements of Saturated Densities and Critical Parameters for the Binary HFO-1234YF + HFC-32 Mixtures," in *International Congress of Refrigeration* (Prague: Czech Republic, 2011).

[33]R. Akasaka, "Thermodynamic property models for the difluoromethane (R-32) + trans-1,3,3,3-tetrafluoropropene (R-1234ze(E)) and difluoromethane + 2,3,3,3-tetrafluoropropene (R-1234yf) mixtures," Fluid Phase Equilib. **358**, 98–104 (2013).

[34]S. L. Outcalt and A. J. Rowane, "Bubble Point Measurements of Mixtures of HFO and HFC Refrigerants," J. Chem. Eng. Data **66**, 4670–4683 (2021).

[35]U. K. Deiters and I. H. Bell, "Calculation of critical curves of fluid mixtures through solution of differential equations," Ind. Eng. Chem. Res. **59**, 19062–19076 (2020).

[36]R. Akasaka, "Thermodynamic property models for the difluoromethane (R-32) + trans-1,3,3,3-tetrafluoropropene (R-1234ze(E)) and difluoromethane + 2,3,3,3-tetrafluoropropene (R-1234yf) mixtures," Fluid Phase Equilib. **358**, 98–104 (2013).

[37]M. R. Moldover and M. O. McLinden, "Using ab initio "data" to accurately determine the fourth density virial coefficient of helium," J. Chem. Thermodyn. **42**, 1193–1203 (2010).

[38]A. Jäger, C. Breitkopf, and M. Richter, "The Representation of Cross Second Virial Coefficients by Multifluid Mixture Models and Other Equations of State," Ind. Eng. Chem. Res. **60**, 9286–9295 (2021).

[39]S. Tomassetti, "pvTz properties of 2,3,3,3-tetrafluoroprop-1-ene + 1,1-difluoroethane binary system measured in the two-phase and superheated vapor regions," Fluid Phase Equilib. **546**, 113173 (2021).

[40]K. Kobayashi, K. Tanaka, and Y. Higashi, "Measurements of the Critical Locus for HFO-1234ze(E) + HFC-32 Mixture," in *The 31st Japan Symposium on Thermophysical Properties* (Fukuoka: Japan, 2010).

[41]K. Kobayashi, K. Tanaka, and Y. Higashi, "PρTx Property Measurements of Binary HFO-1234ze(E) + HFC-32 Refrigerant Mixtures," Nippon Reito Kucho Gakkai Ronbunshu **28**, 415–426 (2011).

[42]K. Tanaka, R. Akasaka, and Y. Higashi, "Measurements of Density and Isobaric Specific Heat Capacity for HFO-1234ze(E)+HFC-32 Mixtures," Nippon Reito Kucho Gakkai Ronbunshu **28**, 427–434 (2011).

[43]K. Yamaya, A. Matsuguchi, and N. Kagawa, "Study on the Isochoric Specific Heat Capacity of a R32+R1234ze(E) Mixture in the Liquid Phase," in *23rd IIR International Congress of Refrigeration* (Prague: Czech Republic, 2011).

[44]T. Jia, S. Bi, X. Hu, X. Meng, and J. Wu, "Volumetric properties of binary mixtures of difluoromethane (R32) + trans-1,3,3,3-tetrafluoropropene (R1234ze(E)) at temperatures from 283.15 K to 363.15 K and pressures up to 100 MPa," J. Chem. Thermodyn. **101**, 54–63 (2016).

[45]S. Tomassetti, U. A. Perera, G. Di Nicola, M. Pierantozzi, Y. Higashi, and K. Thu, "Two-Phase and Vapor-Phase Thermophysical Property (pvTz) Measurements of the Difluoromethane + trans-1,3,3,3-Tetrafluoroprop-1-ene Binary System," J. Chem. Eng. Data **65**, 1554–1564 (2020).

[46]X. Hu, X. Meng, and J. Wu, "Isothermal vapor liquid equilibrium measurements for difluoromethane (R32) + trans-1,3,3,3-tetrafluoropropene (R1234ze(E))," Fluid Phase Equilib. **431**, 58–65 (2017).

[47]L. Kou, Z. Yang, X. Tang, W. Zhang, and J. Lu, "Experimental measurements and correlation of isothermal vapor-liquid equilibria for HFC-32 + HFO-1234ze (E) and HFC-134a + HFO-1234ze (E) binary systems," J. Chem. Thermodyn. **139**, 105798 (2019).

[48]T. Yang, J. I. Siepmann, and J. Wu, "Phase Equilibria of Difluoromethane (R32), 1,1,1,2-Tetrafluoroethane (R134a), and trans-1,3,3,3-Tetrafluoro-1-propene (R1234ze(E)) Probed by Experimental Measurements and Monte Carlo Simulations," Ind. Eng. Chem. Res. **60**, 739–752 (2021).

[49]N. Gao, G. Chen, Y. Wang, and L. Tang, "Experimental isobaric heat capacity of liquid HFC-32 + HFO-1234ze(E) mixture and extension of a predictive corresponding state equation to HFC mixtures," Int. J. Refrig. **88**, 318–323 (2018).

[50]A. J. Rowane and R. A. Perkins, "Speed of Sound Measurements of Binary Mixtures of Hydrofluorocarbons [Pentafluoroethane (R-125), 1,1-Difluoroethane (R-152a), or 1,1,1,2,3,3,3-Heptafluoropropane (R-227ea)] with Hydrofluoroolefins [2,3,3,3-Tetrafluoropropene (R-1234yf) or trans-1,3,3,3-Tetrafluoropropene (R-1234ze(E))]," Int. J. Thermophys. **43**, 127 (2022).

[51]P. Hu, L.-X. Chen, W.-B. Zhu, L. Jia, and Z. Chen, "Isothermal VLE measurements for the binary mixture of 2,3,3,3-tetrafluoroprop-1-ene (HFO-1234yf) + 1,1-difluoroethane (HFC-152a)," Fluid Phase Equilib. **373**, 80–83 (2014).

[52]T. Yang, X. Hu, X. Meng, and J. Wu, "Vapor-Liquid Equilibria for the Binary and Ternary Systems of Difluoromethane (R32), 1,1-Difluoroethane (R152a), and 2,3,3,3-Tetrafluoroprop-1-ene (R1234yf)," J. Chem. Eng. Data **63**, 771–780 (2018).

[53]J. El Abbadi, C. Coquelet, A. Valtz, and C. Houriez, "Experimental measurements and modelling of vapour-liquid equilibria for four mixtures of 2,3,3,3-tetrafluoropropene (R1234yf) with 1,1,1,2-tetrafluoroethane (R134a) or 1,1-difluoroethane (R152a) or trans-1-chloro-3,3,3-trifluoropropene (R1233zd(E)) or 2-chloro-3,3,3-trifluoropropene (R1233xf)," Int. J. Refrig. **140**, 172–185 (2022).

[54]I. H. Bell and E. W. Lemmon, "Automatic Fitting of Binary Interaction Parameters for Multi-fluid Helmholtz-Energy-Explicit Mixture Models," J. Chem. Eng. Data **61**, 3752–3760 (2016).

[55]T. Yang, X. Hu, X. Meng, and J. Wu, "Vapour-liquid equilibria for the binary systems of pentafluoroethane ((R125) + 2,3,3,3-tetrafluoroprop-1-ene (R1234yf)) and (trans-1,3,3,3-tetrafluoropropene R1234ze(E))," J. Chem. Thermodyn. **150**, 106222 (2020).

[56]S. Peng, S. Li, Z. Yang, and Y. Duan, "Vapor-liquid equilibrium measurements for the binary mixtures of pentafluoroethane (R125) with 2,3,3,3-Tetrafluoroprop-1-ene (R1234yf) and 3,3,3-Trifluoropropene (R1243zf)," Int. J. Refrig. **134**, 115–125 (2022).